Available online at www.sciencedirect.com

ScienceDirect

Energy Procedia 8 (2011) 185–192

Energy Procedia

SiliconPV: 17-20 April 2011, Freiburg, Germany

Analysis of the Diffused Front Surface Field of *n*-type Silicon Solar Cells with a-Si/c-Si Heterojunction Rear Emitter

Martin Bivour, Marc Rüdiger, Christian Reichel, Kurt-U. Ritzau, Martin Hermle, Stefan W. Glunz

Fraunhofer Institute for Solar Energy Systems (ISE), Heidenhofstr. 2, 79110 Freiburg, Germany

Abstract

In this work, we focus on the optimization of small-area n^+np^+ *n*-type silicon solar cells featuring an amorphous/crystalline silicon heterojunction (a-Si:H/c-Si SHJ) rear emitter. For cells with a locally c-Si(n^{++}) diffused high-low junction underneath the front side metallization and a full-area c-Si(n^+) diffused front surface field (FSF) in between, efficiencies of up to 20.6 % have been reached. It is shown by experiment and two-dimensional device simulation that when omitting the full-area c-Si(n^+) FSF a sufficient two-dimensional majority carrier transport via the base to the local c-Si(n^{++}) FSF can be secured. For the front side passivation of the c-Si base a stack of thermal SiO_2 / SiN_x and Al_2O_3 / SiN_x was applied.

Keywords: Silicon hetero junction; rear emitter; front surfcace field

1. Introduction

Amorphous/crystalline silicon heterojunction (a-Si:H/c-Si SHJ) solar cells featuring a SHJ at the front and rear side of the solar cell allow open-circuit voltages, V_{oc}, far beyond 700 mV and high efficiencies, η [1]. However, the crucial factor limiting the cell efficiency is the design of the a-Si:H / transparent conductive oxide, TCO, stack at the illuminated front side. For the design of the front SHJ, carrier recombination, carrier transport and the parasitic absorption in the stack have to be considered leading to a complex trade-off between all relevant solar cell output parameters. These correlations become even more complicated when the contact is formed on textured surfaces [2]. In general, for increasing a-Si:H thickness, recombination losses of the SHJ are reduced, leading to an increase in V_{oc} [3]. However, parasitic absorption and the carrier transport are negatively influenced, resulting in a decreased short-circuit current density, J_{sc}, and fill factor, *FF*, respectively. Since the lateral carrier transport to the front

1876–6102 © 2011 Published by Elsevier Ltd. Selection and/or peer-review under responsibility of SiliconPV 2011.
Open access under CC BY-NC-ND license. doi:10.1016/j.egypro.2011.06.122

side metallization can not be realized by the a-Si:H emitter due to the low conductivity, a TCO is required, which also serves as antireflection coating. The TCO must therefore provide optimum electrical and optical properties which are often opposed to one another. Hence, a low parasitic absorption and high conductivity of the TCO [4, 5] as well as a match between the TCO and the a-Si:H work function [6, 7] are further requirements, which must be considered for the optimization of the SHJ. These complex correlations make the optimization of the SHJ, in particular when situated at the illumined front, a very challenging one.

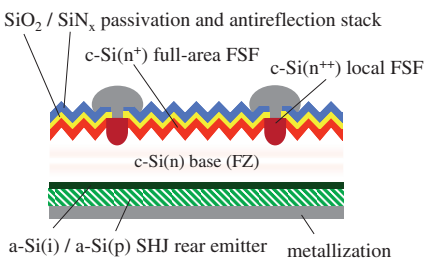

Fig. 1. Schematic cross-section of the n^+np^+ solar cell structure with SHJ rear emitter and diffused FSF.

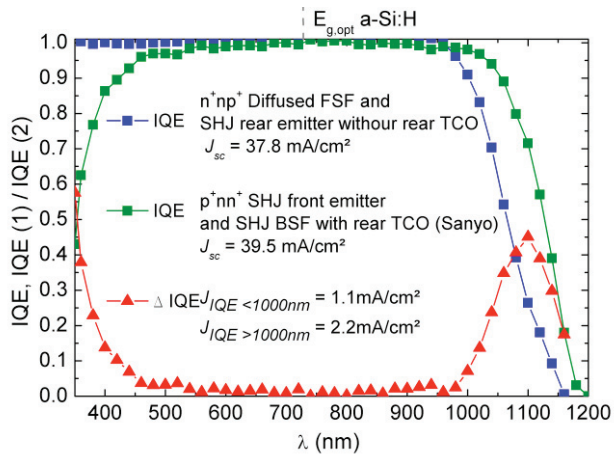

Fig. 2. Comparison of internal quantum efficiency (*IQE*) for a p^+nn^+ full SHJ cells featuring SHJ front emitter and SHJ BSF from Sanyo [8] and for our n^+np^+ cell with a SHJ rear emitter and full-area and local diffused FSF. The wavelength corresponding to the energy of the optical band gap $E_{g,opt}$ of a-Si:H is marked.

To overcome the parasitic absorption, Wünsch *et al.* [9] first introduced a solar cell structure featuring the SHJ only at the rear. A similar cell structure featuring a diffused high-low junction at the front was presented recently [10, 7]. Efficiencies of 19.1 % for a planar *n*-type base (Fig. 1) and 19.8 % for a textured *p*-type base have been achieved so far [7]. Due to the absence of the SHJ at the front, these cells do not show the characteristic parasitic absorption of the front SHJ stack (Fig. 2) and therefore, feature an increased quantum efficiency (*QE*) for wavelengths below 700 nm. In contrast to the excellent front SHJ of Sanyo [8] a current gain of about 1 mA/cm² is achieved for the diffused front surface field (FSF). As a another advantage, the optimization of the SHJ at the rear is clearly simplified since only carrier recombination and transport have to be considered without taking parasitic absorption into account. Furthermore, the SHJ can be formed on a planar surface, which decreases the recombination losses of the SHJ compared to a textured surface. In addition, no TCO at the front is required in terms of lateral majority carrier transport and thus a transparent antireflection coating can be used. Since the TCO layer at the rear is used primarily to increase the rear side reflectance, this layer is not mandatory and allows for a TCO-less SHJ solar cell. Finally, the applied diffused FSF consisting of a locally c-Si(n^{++}) high-low junction underneath the front side metallization and a full-area c-Si(n^+) high-low junction in between is well established and results in high efficiencies [11]. Nevertheless, compared to a SHJ at the front, an increased number of process steps, including high temperature processes, structuring and alignment for the local diffused junction and metallization is required. Promising approaches for process simplification, low temperature metallization and circumventing high temperature processes for junction formation and passivation are being developed [12, 13].

In this paper, we investigate solar cells with and without full-area diffused FSF. By omitting the full-area FSF we are aiming (i) to reduce the number of process steps showing the potential of a substantial simplification of the solar cell fabrication process. Furthermore, (ii) we want to investigate whether or not omitting the diffused full-area high-low junction enables us to further improve the efficiency potential of our front side. On this account, two major requirements have to be met. On the one hand, the absence of the full-area diffusions requires a sufficient 2D carrier transport to the local diffusions underneath the metal contacts which in this case has to be secured only via the base. On the other hand, a front side passivation scheme surpassing the excellent front side passivation quality of the diffused high-low junction (full-area diffused FSF) and the thermal SiO_2 / SiN_x stack is required. In this paper, these requirements are investigated experimentally and by 2D device simulations.

2. Experimental

Fig. 1 shows a schematic cross-section of the investigated 2□2 cm² n^+np^+ solar cells. The cells have been fabricated on front side textured, 200 µm thick, 10 Ω cm, <100> oriented, *n*-type float-zone silicon wafers using a high-efficiency cell process applying photolithography [7]. To ensure a good passivation and a low contact resistance for the majority carrier contact, a deep 20 Ω/□ phosphorus c-Si(n^{++}) diffusion (local FSF) was carried out underneath the front side metallization. The local c-Si(n^{++}) diffusion profile is characterized by a peak surface concentration of about 3□10^{19} cm^{-3} and a depth of about 2 µm. Some cells received an additional deep 150 Ω/□ c-Si(n^+) diffusion (full-area FSF). The c-Si(n^+) diffusion profile is characterized by a peak surface concentration of about 3□10^{18} cm^{-3} and a depth of about 1.2 µm. A stack of 10 nm thermally grown SiO_2 and 60 nm SiN_x deposited by plasma enhanced chemical vapor deposition (PECVD) serves the purposes of passivation and antireflection properties. The cells without full-area FSF received either a 10 nm thermally grown SiO_2 or a 10 nm Al_2O_3 passivation deposited by plasma enhanced atomic layer deposition (PEALD). On top of the SiO_2 or Al_2O_3 layer a 60 nm PECVD SiN_x ARC was deposited. All three front side passivation schemes are characterized by a comparable S_{front} of about 10 cm/s determined from symmetrical lifetime samples fabricated on randomly textured *n*-type float-zone silicon wafers. Further information concerning the a-Si:H(*i*) / a-Si:H(*p*) rear emitter formation can be found in [7].

3. Simulation results and discussion

The 2D device simulations for n^+np^+ solar cells featuring both a full-area FSF and a local FSF (Fig. 3 left) as well as solar cells featuring only a local FSF (Fig. 3 right) have been performed with Sentaurus Device from Synopsys [14]. As input parameters we took the measured diffusion profile and the dimensions of the front side metallization and the local FSF. The width of the local FSF and the metal / semiconductor contact were 8 µm and 5 µm, respectively. For the optical shading a finger width of 25 µm has been used. For the rear emitter an idealized diffused *pn*-junction was assumed in order to focus on the FSF properties and reflecting the efficiency limit given by the front. To account for external series resistance losses a small value of 0.5 Ω cm² was assumed in the simulation. For the simulation study the finger pitch was set to 800 µm, consistent to the fabricated solar cells. Here the influence of the surface recombination velocity at the c-Si front surface $S_{0,front}$ and the base doping concentration N_D for cells with and without diffused full-area FSF on V_{oc}, FF, J_{sc} and η has been investigated. For the dependence of the base carrier lifetime τ_b on N_D, the corresponding Auger lifetime was assumed [15]. It is important to mention that fixed charges in the passivation layer leading to an inversion or accumulation of the c-Si near the surface have not been considered in these simulations.

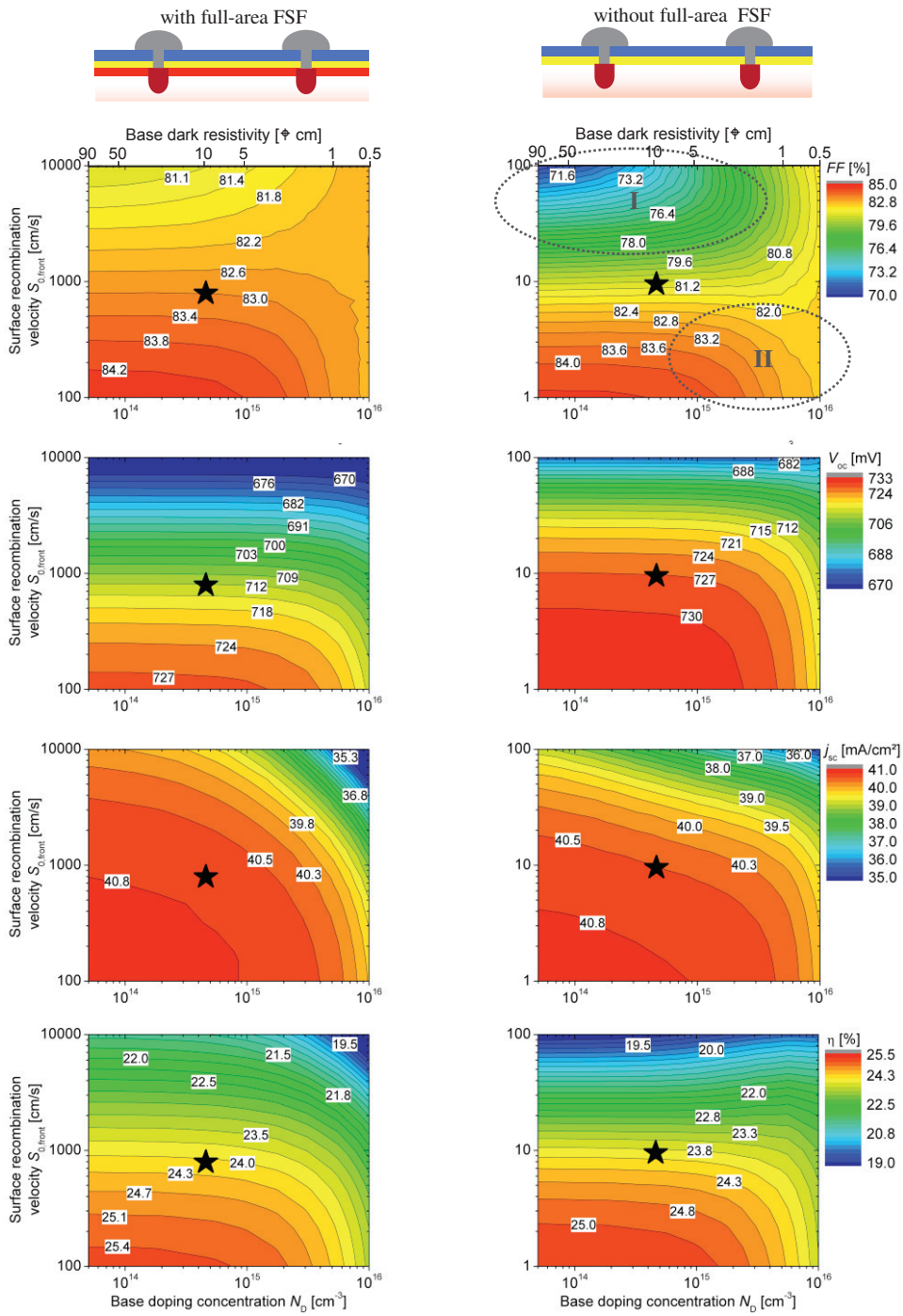

FIG. 3. Simulated influence of N_D and $S_{0,front}$ on FF, V_{oc}, J_{sc} and η of the n^+np^+ SHJ rear emitter cells with and without full-area FSF. The simulated cell parameters corresponding to the experimentally determined N_D and $S_{0,front}$ values ($S_{0,front}$ identical for SiO_2/ SiN_x and Al_2O_3 / SiN_x) are marked by the black star.

Fig. 3 shows the results of the simulations for solar cells with (left) and without (right) full-area FSF. The simulated cell parameters corresponding to the experimentally determined $S_{0,front}$ are marked by the black star.

Regarding the simulated η, it can be seen that for cells with and without full-area FSF comparable η of up to 24 % can be obtained. Taking a closer look at the *FF* reveals that the additional conductivity of the diffused full-area high-low junction is not mandatory to ensure a sufficient 2D majority carrier transport from the base to the local FSF. For very small $S_{0,front}$ and low N_D, comparable *FF* of about 84 % may be theoretically reached with both front sides. However, for the experimentally determined $S_{0,front}$ a lower *FF* of 81 % is observed for the cells without the full-area FSF. For cells with full-area FSF a higher *FF* of 83 % is observed. This difference in *FF* leads to the conclusion that without the full-area FSF, the base alone can not provide sufficient 2D carrier transport to the local FSF. Interestingly, the simulations show that the *FF* of the cells without full-area FSF and the experimentally observed $S_{0,front}$ is independent of the investigated dark resistivity of the base ranging from 0.5 to 90 Ω cm. This can be explained by the decoupling of the base resistivity in the dark and the resistivity under operation conditions, in particular at the maximum power point (MPP). This effect is also known as conductivity modulation [16, 17] and occurs for high-injection conditions in the base. In this case the carrier concentration and therefore the conductivity are significantly increased compared to N_D or the dark conductivity, respectively. Therefore the apparent resistivity of the base is independent of N_D for high-injection conditions. This effect enables a sufficient 2D transport even for dark resistivities as high as 90 Ω cm. For increasing $S_{0,front}$ the carrier concentration and, thus, the apparent base conductivity is reduced and the *FF* is therefore decreased (region I). Hence, a low dark resistivity of the base is only required for an insufficient surface passivation in order to ensure a sufficient 2D majority carrier transport. The decreasing *FF* for increasing N_D in region II is associated with the decrease in τ_b, again leading to a decreased carrier concentration. Nevertheless, the same effect of $S_{0,front}$ (region I) and τ_b (region II) on the *FF* is observed for the cells with full-area FSF although it is less pronounced due to the additional current path given by the diffused high-low junction.

Concerning the front surface passivation quality, it is shown in [18] that the direct passivation of the c-Si base has the potential to outperform the passivation achieved with the diffused high-low junction due to the avoidance of Auger recombination in the diffused regions. This is in agreement with the simulations where, for the experimentally determined $S_{0,front}$, a V_{oc} gain of about 15 mV and the same high J_{sc} level of above 40 mA/cm² for the cells without-full area diffused FSF are observed.

4. Experimental solar cell results and discussion

In Table 1 the experimental cell results for the three different front sides under investigation are shown. It can be observed that for cells featuring a full-area diffused FSF between the local diffused FSF (Fig. 1) and a SiO_2 / SiN_x stack the highest η´s have been reached. In general, the SHJ rear emitter limits V_{oc} and *FF* for all three types of cells to 690 mV and 80%, respectively. Therefore the high V_{oc} and *FF* potential of the front sides can not be shown here. Furthermore, J_{sc} for all solar cells is limited to 38 mA/cm² due to a poor rear side reflection, causing a low *IQE* for > 1000 nm (see Fig. 2).

For the best cells without a full-area FSF where a SiO_2 / SiN_x stack is used to directly passivate the lowly-doped c-Si base the *FF* is not negatively affected. This leads to the conclusion that without the full-area FSF a sufficient 2D carrier transport to the local front side contacts can be secured via the base. Additionally, a comparable J_{sc} and *IQE* (Fig. 4) as for the cells with full-area FSF and the SiO_2 / SiN_x stack is observed, indicating a comparable front side passivation quality at least under short-circuit

Table 1. Parameters of 2x2cm² solar cells with the highest efficiency and 10 Ω cm *n*-typ base (corresponding $S_{0,front}$

determined from textured lifetime samples are also shown)

front side passivation	S_{front} (cm/s)	V_{oc} (mV)	J_{sc} (mA/cm^2)	*FF* (%)	η (%)
full-area FSF + **SiO_2** / SiN_x	$S_0 = 800$, $S_{eff} = 10$	688	37.8	79.4	20.6
without full-area FSF + **SiO_2** / SiN_x	$S_0 = 10$	656	38.1	79.3	19.8
without full-area FSF + **Al_2O_3** / SiN_x	$S_0 = 10$	650	35.2	75.5	17.3

conditions. However, a clear trend towards a lower V_{oc} is observed for the cells without full-area FSF, limiting the η to below 20 %. The increased front side recombination under open-circuit conditions for the cells without a full-area FSF was not expected from the simulations or from the S_0 values determined from lifetime samples (see Tab. 1) and must be further investigated. Furthermore, the influence of a possible accumulation layer introduced by the SiN_x [19, 20, 21] on the solar cell performance has to be taken into account.

For the cells without a full-area FSF where an Al_2O_3 / SiN_x stack was used for front side passivation a significant decrease in *FF*, J_{sc} and V_{oc} is observed. In addition, a distinctive bias illumination dependence of the *IQE* and a lower absolute *IQE* level at one sun bias illumination is observed. The decreased performance of the cells with Al_2O_3 / SiN_x front side passivation is attributed to the high density of fixed negative charges of the Al_2O_3 causing an inversion layer, which acts as a floating junction, in the lowly-doped base. In this case, field effect passivation is the dominant passivation mechanism leading to an injection-dependent passivation of the *n*-type base by Al_2O_3 [22]. This results in an increased front side recombination for lower carrier concentrations. This is a general observation for passivation by an inversion layer [23, 24, 25] and explains the strong injection (bias illumination) dependence of the *IQE*. However, a decrease of the device performance due to parasitic shunting of the floating junction with the front side metallization should be suppressed by the local c-Si(n^{++}) FSF diffusions underneath the metallization [26], but cannot be fully excluded. In Fig. 4 it can be seen that without bias illumination (0 suns) no significant surface passivation is reached, resulting in an *IQE* of nearly zero for below 800 nm. In contrast for increasing illumination and, therefore, carrier concentration the front side passivation and thus the *IQE* is improved. This dependence is not observed for the cells with full-area FSF and SiO_2 / SiN_x passivation and only to a small extent for the cells without full-area FSF and SiO_2 / SiN_x passivation ([24] for further informations). Summing up it can be stated that on device level, Al_2O_3 is inadequate for the passivation of the lowly-doped *n*-type base for the investigated n^+np^+ cell structure.

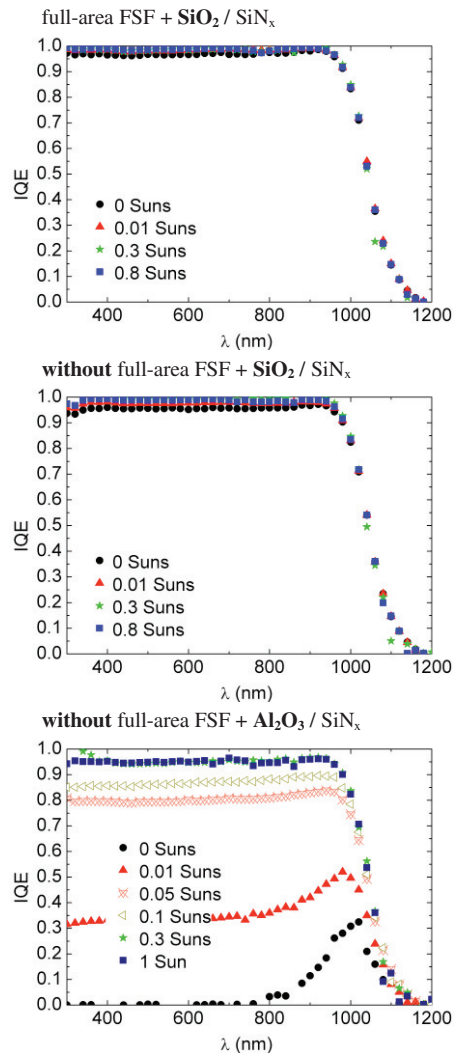

Fig. 4. Bias illumination dependent *IQE* for the three front side passivation schemes.

5. Conclusion

It was demonstrated that by omitting the diffused full-area FSF an excellent surface passivation of the c-Si base throughout all

solar cell operation conditions is mandatory to maintain a sufficient passivation and 2D carrier transport. These requirements are not fulfilled for the Al_2O_3 / SiN_x passivation stack due to the inversion layer introduced by Al_2O_3. For the solar cells featuring a SiO_2 / SiN_x passivation stack a sufficient passivation and 2D transport is ensured for short-circuit and MPP condition and therefore no influence in J_{sc} and *FF* is observed for omitting the full-area diffused FSF. However, recombination at open-circuit is increased compared to the cells featuring a full-area diffused FSF limiting the solar cell η to 19.8%. Therefore further investigations for the implementation of alternative high-quality front side passivation schemes are required. For cells featuring a diffused full-area FSF lower front side recombination at open-circuit is observed leading to the highest η of 20.6%. We are confident that by electrical and optical optimization of the SHJ rear emitter stack a further η gain is within reach.

Acknowledgements

This work was funded by the German Federal Ministry for the Environment. Nature Conservation and Nuclear Safety under contract number 0329849A “Th-ETA”. M. Bivour gratefully acknowledges the scholarship support from the Reiner Lemoine Stiftung.

References

[1] Taguchi M, Tsunomura Y, Inoue H, Taira S, Nakashima T, Baba T, *et al.*. High-Efficiency HIT Solar Cell on Thin (<100μm) Silicon Wafer, *Proc. 24th EU PVSEC*, Hamburg, Germany, p. 1690-3 (2009).

[2] Olibet S, Monachon C, Hessler-Wyser A, Vallat-Sauvain E, De Wolf S, Fesquet L, *et al*.. Textured Silicon Heterojunction Solar Cells with over 700 mV Open-Circuit Voltage Studied by Transmission Electron Microscopy, *Proc. 23rd EU PVSEC*, Valencia, Spain, p. 1140-4 (2008)

[3] Fujiwara H, Kondo M. Effects of a-Si:H layer thicknesses on the performance of a-Si:H/c-Si heterojunction solar cells, *J. Appl. Phys.* ***101***, 054516, (2007).

[4] Choong G, Bôle B, Barraud L, Zicarelli F, Descoeudres A, De Wolf S, *et al.*. Transparent Concuctive Oxides for Silicon Heterojunction Solar Cells, *Proc. 25th EU PVSEC*, Valencia, Spain, p. 2505-10 (2010).

[5] Koida T, Fujiwara H, Kondo M. High-mobility hydrogen-doped In_2O_3 transparent conductive oxide for a-Si:H/c-Si heterojunction solar cells”, *Solar Energy Materials & Solar Cells* ***93***, Issues 6-7, p. 851-4 (2009).

[6] Kim J, Abou-Kandil A, Fogel K, Hovel H, Sadana DK. The role of high work-function metallic nanodots on the performance of a-Si:H solar cells: offering ohmic contact to light trapping, *ACS Nano* ***4*** (12), p. 7331-6 (2010).

[7] Bivour M, Meinhardt C, Pysch D, Reichel C, Ritzau KU, Hermle M, Glunz SW. N-type Silicon Solar Cells with Amorphous/Crystalline Silicon Heterojunction Rear Emitter” *Proc. 35th IEEE PVSC*, Honolulu, USA, p. 1304-8 (2010).

[8] Fujishima D, Inoue H, Tsunomura Y, Asaumi T, Taira S, Kinoshita T, *et al.*. High-Performance HIT Solar Cells for Thinner Silicon Wafers, *Proc. 35th IEEE PVSC*, Honolulu, USA, p. 3137-40 (2010).

[9] Wunsch F, Citarella G, Abdallah O, Kunst M. An inverted a-Si:H/c-Si hetero-junction for solar energy conversion”, *J. of Non-Crystalline Solids* ***352***, Issues 9-20, p. 1962-6 (2006).

[10] Matsumoto Y, Ortega M, Sánchez VM, Wünsch F, Urbano JA. HW-CVD Deposited μc-Si:H for the Inverted Heterojunction Solar Cell, *Proc. 35th IEEE PVSC*, Honolulu, USA, p. 1450-5 (2010).

[11]Zhao J, Wang A. High Efficiency Rear Emitter Pert Cells on CZ and FZ N-Type Silicon Substrates”, *Proc. 4th IEEE World Conference*, Waikoloa, USA, p. 996-9 (2006).

[12] Kray D, Alemán M, Fell A, Hopman S, Mayer K, Mesec M, *et al.*. Laser-doped Silicon Solar Cells by Laser Chemical Processing (LCP) Exceeding 20% Efficiency, *Proc. 33rd IEEE PVSC*, St. Diego, USA, DOI: 10.1109/PVSC.2008.4922848 (2008).

[13] Bock R, Mau S, Schmidt J, Brendel R. Back-junction back-contact n-type silicon solar cells with screen-printed aluminum-alloyed emitter, *Appl. Phys. Lett.* ***96*** (26), 263507 (2010).

[14] Sentaurus, TCAD, release E2010.12

[15] Rüdiger M, Schmiga C, Rauer M, Hermle M, Glunz SW. Optimisation of Industrial n-type Silicon Solar Cells with Aluminium-Alloyed Rear Emitter by Means of 2D Numerical Simulation, *Proc. 25th EU PVSEC*, Valencia, Spain, p. 2280-6 (2010).

[16] Cid M, Ruiz JM. Study of Injection Effects on BSF Silicon Solar Cells, *IEEE T-ED* ***36*** (3), p. 507-13 (1989).
[17] Granek F, Hermle M, Huljic DM, Schultz-Wittmann O, Glunz SW. Enhanced lateral current transport via the front N^+ diffused layer of N-type high-efficiency back-junction back-contact silicon solar cells, *Prog. in Photovolt.: Res. Appl.* ***17*** (1), p. 47-56, (2009).
[18] Granek F, Reichel C, Hermle M, Huljić DM, Schultz O, Glunz SW. Front Surface Passivation of n-type High-Efficiency Back-Junction Silicon Solar Cells using Front Surface Fields, *Proc. 22nd EU PVSEC*, Milan, Italy, p. 1262-5 (2007).
[19] Kuhlmann B, Aberle AG, Meyer R, Hubner A, Hampe C, Hezel R. Fabrication and characterisation of 662-mV open-circuit voltage high-efficiency inversion-layer silicon solar cells, *Proc. 25th IEEE PVSC*, Washington DC, USA, p. 493-6 (1996).
[20] Martin I, Lövblom R, Alcubilla R. High-Efficiency Solar Cells based on Inversion Layer Emitters, *Proc. 24th EU PVSEC*, Hamburg, Germany, p. 1985-91 (2009).
[21] Schmidt J, Merkle A, Hoex B, van de Sanden MCM, Kessels WMM, Brendel R. Atomic-layer-deposited aluminum oxide for the surface passivation of high-efficiency silicon solar cells, *Proc. 33rd IEEE PVSC*, San Diego, CA, USA, DOI: 10.1109/PVSC.2008.4922636 (2008).
[22] Hoex B, Schmidt J, Pohl P, van de Sanden MCM, Kessels WMM. Silicon surface passivation by atomic layer deposited Al_2O_3, J. Appl. Phys. 104 (4), 044903 (2008).
[23] Glunz S. W, Biro D, Rein S, Warta W, Field-effect passivation of the SiO2Si interface , J. Appl. Phys. 86, 683 (1999)
[24] Granek F, Hermle M, Glunz SW. Analysis of the current linearity at low illumination of high-efficiency back-junction back-contact silicon solar cells, *Phys. Stat. Solidi – RRL* ***2*** (4), p. 151-3 (2008).
[25] Dauwe, S., Mittelstädt, L., Metz, A. and Hezel, R. Experimental evidence of parasitic shunting in silicon nitride rear surface passivated solar cells, *Progress in Photovoltaics: Research and Applications*, 10: 271–278. (2002)
[26] Dauwe, S.; Mittelstadt, L.; Metz, A.; Schmidt, J.; Hezel, R. Low-temperature rear surface passivation schemes for >20% efficient silicon solar cells, *, 2003. Proc. of 3rd World Conference on Photovoltaic Energy Conversion* , Osaka, Japan, p.1395-1398 (2003)